Time-resolved view on charge-resonance-enhanced ionization

Norio Takemoto* and Andreas Becker

JILA and Department of Physics, University of Colorado, 440 UCB, Boulder, Colorado 80309-0440, USA

(Received 18 April 2011; published 3 August 2011)

We theoretically investigate the electronic dynamics in the hydrogen molecular ion at fixed intermediate internuclear distances in two-dimensional space for the electron in a linearly polarized laser field. Our results of numerical simulations confirm the predictions of multiple bursts of ionization within a half cycle of the laser field oscillation as recently reported for one-dimensional models. Based on the analysis of the Floquet states for a two-state model of the molecular ion, we discuss the relation of the multiple ionization bursts to the so-called charge-resonance-enhanced ionization phenomenon and the momentum gates.

DOI: 10.1103/PhysRevA.84.023401 PACS number(s): 32.80.Rm, 33.80.Rv

I. INTRODUCTION

Ionization of atoms and molecules is an important process in strong-field physics. The free electron is detected with discrete kinetic energies, which is known as above-threshold ionization [1]. Ionization is also the initial step for many other phenomena occurring in the interaction of matter with intense laser pulses since the electron can be driven back to the parent ion by the strong field. This leads to the generation of higher-order harmonics [2] or the release of a second electron, known as nonsequential double ionization [3]. Also, the generation of attosecond pulses, which are used to image and control the ultrafast electron dynamics in atoms and molecules on its natural time scale [4,5], is related to an initial ionization step.

The ionization process in intense laser fields has often been understood by the quasistatic tunnel ionization picture. In this popular picture the laser field is approximated as a static electric field at each instant of time and the electron is considered to quickly tunnel through (or leave over) the barrier created by the combined potentials of the laser field and the Coulomb attraction of the core. It leads to the expectation that the ionization rate is at maximum whenever the barrier becomes the thinnest (and lowest), which coincides at the field maxima. This prediction is in agreement with recent attosecond time-resolved observation for ionization of Ne^+ [6]. Even in the case of nonadiabatic tunnel ionization, in which the laser field is considered to change significantly while the electron is escaping from the attractive potential of the core, the ionization rate exhibits a single maximum during each half-cycle of the laser field oscillation [7].

In contrast to these popular assumptions, our recent results of numerical simulations on model systems of $H_2{}^+$ interacting with intense laser fields indicate that in this simplest molecule there can be multiple bursts of ionization within a half cycle of the laser field [8,9]. These bursts are related to a transient electron localization at one of the protons on the attosecond time scale [10,11]. The subcycle oscillation of the electron density occurs in $H_2{}^+$ after the molecular ion has stretched to intermediate internuclear distances. It is due to a trapping of the electron population in a pair of so-called charge-resonance (CR) states [12,13], which is, in our case, the energetically lowest σ_g and σ_u states of $H_2{}^+$. It is likely that similar attosecond intramolecular electron dynamics and related multiple ionization bursts (MIBs) appear in other molecules with CR states as well.

Here we further explore this phenomenon in view of the following aspects: First, in our previous investigations of the MIBs in $H_2{}^+$ [8,9], we employed models in which the electronic motion is restricted along the electric field vector of a linearly polarized laser field. Below we show that the attosecond intramolecular electron dynamics and the MIBs are not caused by this restriction. Results of numerical simulations of the electron dynamics in two degrees of freedom confirm our previous predictions. Second, we show how the MIBs are related to the well-known mechanism of charge-resonance-enhanced ionization (CREI) [14,15], in which the electron is efficiently ionized from the uphill potential. To this end, we analyze the dynamics in a two-state model (consisting of the two CR states) using a series expansion of the Floquet states [16]. We show that the first-order term of this expansion represents the transient intramolecular electron transfer on the sub-laser-cycle time scale. The ionization current of the CREI process is modulated by this ultrafast electron transfer. Furthermore, we elucidate in the Wigner representation that this bunching of the ionization current from the upper hill is regulated via the previously introduced concept of momentum gates [11]. In this sense, the MIBs do not replace CREI, but both phenomena coexist. The MIBs can be viewed as a refined, time-resolved version of the CREI picture.

The rest of the paper is organized as follows. In Sec. II, we present the results of numerical simulations using different models of $H_2{}^+$ in order to show that the sub-laser-cycle electron dynamics in the molecular ion and the MIBs do not depend on the details of the model used for the calculations. We then introduce the two-state model and analyze it in terms of the Floquet states in Sec. III. Finally, we show and discuss in Sec. IV the relation of the MIBs to the well-known CREI mechanism and the concept of momentum gates. The paper ends with conclusions.

II. SUBCYCLE ELECTRON DYNAMICS IN $H_2{}^+$

In our previous numerical simulations [8], we used two different models of $H_2{}^+$, in both of which the electronic motion

*Present address: Department of Chemical Physics, Weizmann Institute of Science, IL-76100 Rehovot, Israel; norio.takemoto@weizmann.ac.il

was restricted along the polarization direction of the laser field. Results for the temporal evolution of the electron densities for the cases that the protons were either fixed in space or allowed to move along the polarization direction were in very good agreement with each other. We thus concluded that the nonadiabatic coupling of the nuclear and electronic motions is not essential for the formation of the MIBs. In this article, we now investigate the influence of the transverse degree of freedom on the localization of the electron at one of the two protons and the MIBs.

A. Numerical models

We consider the electronic motion in a model for $H_2{}^+$, in which the two protons are aligned along the polarization direction of linearly polarized laser light and their distance is fixed at R_0. The Hamiltonian of this system can be given as (Hartree atomic units, $e = m = \hbar = 1$, are used throughout the article, unless otherwise noted)

$$H^{(2D)}(t) = -\frac{1}{2}\left(\frac{1}{\rho}\frac{\partial}{\partial\rho}\rho\frac{\partial}{\partial\rho} + \frac{\partial^2}{\partial z^2}\right) - \frac{1}{\sqrt{\rho^2 + \left(z + \frac{R_0}{2}\right)^2}} - \frac{1}{\sqrt{\rho^2 + \left(z - \frac{R_0}{2}\right)^2}} + zE(t), \quad (1)$$

where ρ and z are the transverse and longitudinal coordinates of the electron, respectively, and $E(t) = -dA(t)/dt$ is the laser electric field. The laser pulse was assumed to have a $\sin^2$ envelope for the vector potential,

$$A(t) = f_A(t)\sin(\omega t + \varphi), \quad (2)$$

$$f_A(t) = \begin{cases} A_0 \sin^2\left[\pi\left(t + \frac{T}{2}\right)/T\right] : -T/2 \leqslant t \leqslant T/2, \\ 0 \qquad\qquad\qquad\quad ,\text{otherwise}. \end{cases} \quad (3)$$

The Hamiltonian operator in Eq. (1) was discretized on the two-dimensional (2D) grid such that the resultant Hamiltonian matrix is Hermitian and the wave function propagator becomes unitary [17–19]. To this end, the grid points in ρ were set with an offset of half an interval from $\rho = 0$ as $\{\Delta\rho/2, 3\Delta\rho/2, \ldots, (2N_\rho - 1)\Delta\rho/2\}$. In this way any numerical instability due to the singularity of the Coulomb potential in Eq. (1) at $(\rho, z) = (0, \pm R_0/2)$ was avoided as well. The internuclear distance R_0 was fixed at 7. By distributing the grid points over $0 < \rho < 15$ and $-40 < z < 40$ at the intervals of $\Delta\rho = 0.0375$ and $\Delta z = 0.1$, respectively, and setting the time step as $\Delta t = 0.01$, the ground and first excited states were obtained by imaginary time propagation at the energies of -0.648 and -0.639, respectively (not including the $1/R_0$ repulsion). The transition dipole moment between these two states was $d_{gu} = 3.40$.

To investigate the influence of the transverse degree of freedom on the intramolecular electron dynamics, we also obtained results from the previously used fixed-nuclei one-dimensional (1D) model, in which the motion of the electron is restricted along the polarization direction. The corresponding Hamiltonian is given by

$$H^{(1D)}(t) = -\frac{1}{2}\frac{\partial^2}{\partial z^2} - \frac{1}{\sqrt{\left(z + \frac{R_0}{2}\right)^2 + a_e}} - \frac{1}{\sqrt{\left(z - \frac{R_0}{2}\right)^2 + a_e}} + zE(t), \quad (4)$$

with the soft-core parameter $a_e = 1.0$ [8]. The grid points were chosen over $-300 < z < 300$ at the interval of $\Delta z = 0.0732$, and the time step of the wave function propagation was set at $\Delta t = 0.0168$. The ground- and first-excited-state energies of this model were -0.823 and -0.810, respectively, and the transition dipole moment was 3.36.

B. Time evolution of the electron density

For our exemplary comparison of the evolution of the electron density, we prepared the system in the respective ground state of the two models and propagated the wave function under the same laser pulse of peak intensity $I_0 = 6 \times 10^{13}$ W/cm^2, wavelength $\lambda = 800$ nm, pulse duration of 10 cycles [full width at half maximum (FWHM)], and carrier-to-envelope phase $\varphi = \pi/2$. The electron density obtained using the two models are compared in Fig. 1 over the central laser cycle at the peak of the laser pulse. The vector potential and the electric field of the applied laser pulse are shown in panel (d) for comparison.

Figures 1(a) and 1(b) show the electron densities in the 1D and 2D models, respectively, on a logarithmic scale. For the sake of comparison, the electron density $|\Psi^{(2D)}(\rho, z, t)|^2$ in the 2D model was integrated over the transverse direction as

$$P(z, t; \rho_d) = \int_0^{\rho_d} d\rho\ \rho |\Psi^{(2D)}(\rho, z, t)|^2, \quad (5)$$

with $\rho_d = 0.5$. As can be seen from the comparison, the time evolution of the electron density in the 2D model exhibits

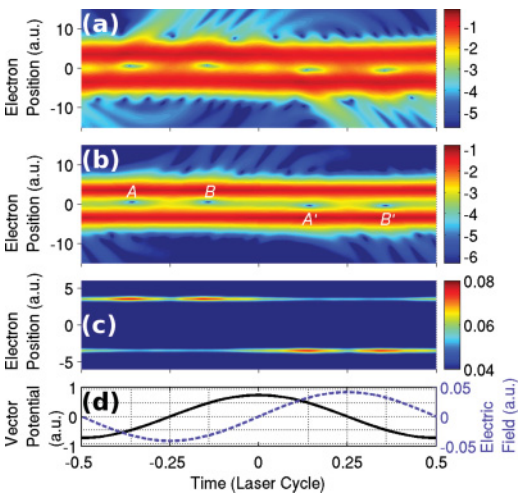

FIG. 1. (Color online) Time evolution of the electron density along the molecular axis obtained by (a) 1D model and (b) 2D model with $R_0 = 7$ are plotted on logarithmic scale. Laser pulse of intensity 6×10^{13} W/cm^2, wavelength 800 nm, and FWHM duration of 10 laser cycles were used. (c) The electron density in the 2D model plotted on linear scale. (d) The vector potential $A(t)$ (black solid line) and the electric field $E(t)$ (blue dashed line) of the laser pulse.

qualitatively the same behavior as that in the 1D model. For the present laser parameters there are two bursts of ionization within a half cycle of the laser field as marked by A, B, A', and B' in Fig. 1(b). The subcycle transient electron localization becomes even more obvious if the electron density is plotted on a linear scale, as shown in Fig. 1(c) for the 2D model. The results also confirm that it is the electron localization which induces the MIBs. These major bursts are further divided into finer fringes at $|z| \gtrsim 8$ due to interferences with the rescattering wave packet, which was emitted in the previous half cycle and now returns to the molecular core, as shown in Ref. [9]. Thus, from this exemplary comparison we may conclude that the subcycle intramolecular electron dynamics and the MIBs are not a peculiarity of the previously used 1D model, but they should be present in the actual 3D molecular ion as well.

III. TWO-STATE ANALYSIS

A. Localized states of charge-resonance pair

In order to further investigate the electron dynamics, we make use of a simple two-state model in which just the two energetically lowest states of H_2^+ are considered. The ground state, $|g\rangle$, and the first excited state, $|u\rangle$, of H_2^+ at $R_0 = 7$ are almost degenerate, and their superpositions form the states localized at the respective protons,

$$|L\rangle = \frac{1}{\sqrt{2}}(|g\rangle + |u\rangle), \tag{6}$$

$$|R\rangle = \frac{1}{\sqrt{2}}(|g\rangle - |u\rangle). \tag{7}$$

Without loss of generality, we set the overall phases of $\langle z|g\rangle$ and $\langle z|u\rangle$ such that $\langle z|L\rangle$ and $\langle z|R\rangle$ are localized at $z < 0$ and $z > 0$, respectively. Conversely, the ground and first excited states may be considered as gerade and ungerade superpositions of these two localized states. Thus, when the $|g\rangle$ and $|u\rangle$ are mixed under the influence of an external field, the electron density can oscillate between the two protons, giving rise to a large transition dipole moment between these two states, $d_{gu} = \langle g|(-z)|u\rangle \sim R_0/2$, along the molecular axis at large internuclear distance R_0 [12,20,21]. Due to this strong coupling, the population of the system is expected to be essentially trapped within this pair of lowest CR states before ionization.

We extracted the populations in the lowest CR states from the solution $|\Psi\rangle$ of the time-dependent Schrödinger equation (TDSE) obtained by the numerical simulations by projection to the localized states $|L\rangle$ and $|R\rangle$. Figure 2(b) shows the normalized local populations

$$P_L = \frac{|\langle L|\Psi\rangle|^2}{|\langle L|\Psi\rangle|^2 + |\langle R|\Psi\rangle|^2}, \tag{8}$$

$$P_R = \frac{|\langle R|\Psi\rangle|^2}{|\langle L|\Psi\rangle|^2 + |\langle R|\Psi\rangle|^2}, \tag{9}$$

in the 2D model, whereas in Fig. 2(a) we present the same quantities for the 1D model. The results clearly show the transient electron localization seen in Fig. 1(c), and therefore confirm that their origin can be analyzed in the two-state model for the present laser parameters.

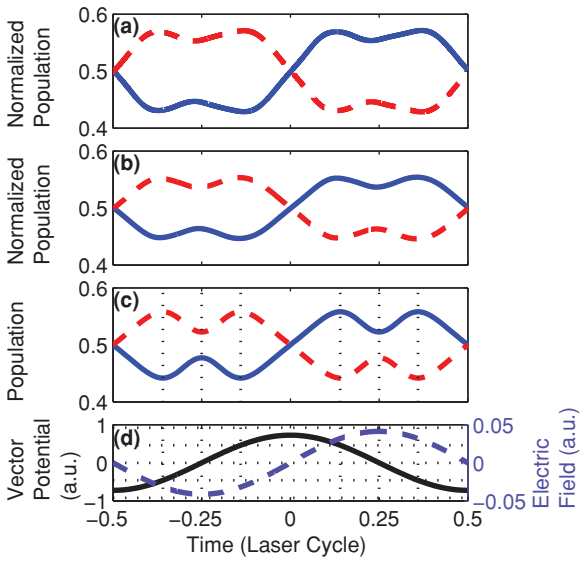

FIG. 2. (Color online) Population analysis in the lowest CR pair. (a) Normalized populations P_L (blue solid line) and P_R (red dashed line) in the 1D model. (b) Same as in panel (a), except in 2D model. (c) Same as panels (a) and (b), except that the populations are obtained by Floquet analysis. (d) Vector potential (black solid line) and electric field (blue dashed line) of the applied laser pulse.

B. Series expansion of Floquet states

By approximating the laser field as a cw field, the Floquet states of the two-level system can be obtained in a form of a series expansion [16,22,23]. Following the analysis in Ref. [16] we write the Hamiltonian of the two-level system as

$$H^{(2lev)}(t) = \frac{\Delta_0}{2}[\sigma_{uu} - \sigma_{gg}] - d_{gu}E(t)[\sigma_{gu} + \sigma_{ug}], \tag{10}$$

where $\Delta_0 > 0$ is the energy difference between $|u\rangle$ and $|g\rangle$, $d_{gu} = \langle g|(-z)|u\rangle$ is the transition dipole matrix element, and $\sigma_{ij} = |i\rangle\langle j|$ $(i,j \in \{g,u\})$. The origin of the potential energy is taken at the center of the energy levels of $|g\rangle$ and $|u\rangle$. We assume a cw laser field whose vector potential is given as

$$A(t) = A_0 \sin(\omega t + \varphi) + \tilde{A}, \tag{11}$$

where $\tilde{A}$ is an arbitrary constant defining the origin of the vector potential whose value does not affect any observable. The electric field is related to the vector potential as

$$E(t) = -\frac{dA(t)}{dt} = -E_0 \cos(\omega t + \varphi), \tag{12}$$

where $E_0 = \omega A_0$. By introducing a dimensionless time coordinate,

$$\tau := \omega t + \varphi, \tag{13}$$

the two-level TDSE can be written as

$$i\frac{\partial}{\partial \tau}|\Psi^{(2lev)}(\tau)\rangle = \bar{H}^{(2lev)}(\tau)|\Psi^{(2lev)}(\tau)\rangle, \tag{14}$$

where $\bar{H}^{(2lev)}(\tau) = H^{(2lev)}(t(\tau))/\omega$.

Due to the periodicity of the Hamiltonian $\bar{H}^{(2lev)}(\tau) = \bar{H}^{(2lev)}(\tau + 2\pi)$, according to the Floquet theorem, the TDSE (14) has the following form of special solutions:

$$\left|\Psi_j^{(2lev)}(\tau)\right\rangle = \exp(-i\epsilon_j\tau)\left|\varphi_j^F(\tau)\right\rangle, \quad j = 1,2, \tag{15}$$

where the quasienergies $\{\epsilon_j\}$ and Floquet eigenvectors $\{|\varphi_j^{\rm F}(\tau)\rangle\}$ are the eigenvalues and eigenstates of the Schrödinger operator,

$$\left(\bar{H}^{(2{\rm lev})}(\tau) - i\frac{\partial}{\partial\tau}\right)|\varphi_j^{\rm F}(\tau)\rangle = \epsilon_j|\varphi_j^{\rm F}(\tau)\rangle. \tag{16}$$

When the laser frequency ω is much larger than the transition frequency Δ_0 between $|{\rm g}\rangle$ and $|{\rm u}\rangle$ and/or the laser-induced coupling is strong, the quasienergies can be expanded as [16]

$$\epsilon_1 = -\frac{\Delta_0}{2\omega}J_0(\zeta)[1+O(\varepsilon^2)], \tag{17}$$

$$\epsilon_2 = \frac{\Delta_0}{2\omega}J_0(\zeta)[1+O(\varepsilon^2)], \tag{18}$$

where $J_n(\zeta)$ represents the nth-order Bessel function of the first kind, $\zeta = 2d_{\rm gu}E_0/\omega = 2d_{\rm gu}A_0$ is proportional to the ratio of the Rabi frequency to the laser frequency, and the perturbation parameter ε can be taken as either $\varepsilon = \Delta_0/\omega$ or $\varepsilon = \Delta_0/\sqrt{\omega d_{\rm gu}E_0}$. The corresponding Floquet states are then given by (for a comprehensive derivation, please see Ref. [16])

$$\begin{aligned}|\varphi_1^{\rm F}(\tau)\rangle = &\left[\cos\phi(\tau) + i\frac{\Delta_0}{\omega}\cos\phi(\tau)\xi_{\rm s}(\tau)\right.\\ &\left.+ i\frac{\Delta_0}{\omega}\sin\phi(\tau)\xi_{\rm a}(\tau)\right]|{\rm g}\rangle\\ &+\left[i\sin\phi(\tau) + \frac{\Delta_0}{\omega}\cos\phi(\tau)\xi_{\rm a}(\tau)\right.\\ &\left.-\frac{\Delta_0}{\omega}\sin\phi(\tau)\xi_{\rm s}(\tau)\right]|{\rm u}\rangle + O(\varepsilon^2)\end{aligned} \tag{19}$$

and

$$\begin{aligned}|\varphi_2^{\rm F}(\tau)\rangle = &\left[i\sin\phi(\tau) - \frac{\Delta_0}{\omega}\cos\phi(\tau)\xi_{\rm a}(\tau)\right.\\ &\left.+\frac{\Delta_0}{\omega}\sin\phi(\tau)\xi_{\rm s}(\tau)\right]|{\rm g}\rangle\\ &+\left[\cos\phi(\tau) - i\frac{\Delta_0}{\omega}\cos\phi(\tau)\xi_{\rm s}(\tau)\right.\\ &\left.-i\frac{\Delta_0}{\omega}\sin\phi(\tau)\xi_{\rm a}(\tau)\right]|{\rm u}\rangle + O(\varepsilon^2),\end{aligned} \tag{20}$$

where

$$\phi(\tau) = -d_{\rm gu}[A(t(\tau)) - \tilde{A}], \tag{21}$$

$$\xi_{\rm s}(\tau) = \sum_{k=1}^{\infty}J_{2k}(\zeta)\frac{\sin[2k\tau]}{2k}, \tag{22}$$

$$\xi_{\rm a}(\tau) = \sum_{k=0}^{\infty}J_{2k+1}(\zeta)\frac{\cos[(2k+1)\tau]}{2k+1}. \tag{23}$$

For our present 2D model system, the perturbation parameters were either $\Delta_0/\omega = 0.164$ or $\Delta_0/\sqrt{\omega d_{gu}E_0} = 0.105$ in the laser field of wavelength 800 nm and intensity 6×10^{13} W/cm^2. In Fig. 3, we compare the quasienergies calculated from the series expansion formulas (17) and (18) with the values obtained by numerically solving the eigenvalue equation (16). The two results agree with each other very well, indicating that the contributions of the terms beyond the first-order term in the expansion are negligible.

C. Time evolution of local population

Before the emergence of the attosecond pulse technology, the Floquet states were often used to analyze the laser-matter interaction over many cycles in terms of the lifetime of a metastable state [24–28] or the light-dressed electronic potentials [29,30]. In contrast, we use the Floquet solutions to investigate the dynamics of the system on a sub-laser-cycle time scale. This analysis is valid if the electric field amplitude E_0 does not change significantly within one laser cycle.

The general solution of the two-state TDSE (14) can be expressed as a superposition of the two special solutions in Eq. (15), that is,

$$\begin{aligned}|\Psi^{(2{\rm lev})}(\tau)\rangle = &\, c_1\exp(-i\epsilon_1\tau)|\varphi_1^{\rm F}(\tau)\rangle\\ &+c_2\exp(-i\epsilon_2\tau)|\varphi_2^{\rm F}(\tau)\rangle,\end{aligned} \tag{24}$$

where the coefficients c_j $(j=1,2)$ are constant in time. Therefore, by projecting $|\Psi^{(2{\rm lev})}(\tau)\rangle$ to $|{\rm L}\rangle$ and $|{\rm R}\rangle$, the time evolution of the local populations are expressed as [using Eqs. (19) and (20)]

$$|\langle{\rm L}|\Psi^{(2{\rm lev})}(\tau)\rangle|^2 = \tfrac{1}{2}|c_1+c_2|^2 + \Delta P^{(1)} + O(\varepsilon^2), \tag{25}$$

$$|\langle{\rm R}|\Psi^{(2{\rm lev})}(\tau)\rangle|^2 = \tfrac{1}{2}|c_1-c_2|^2 - \Delta P^{(1)} + O(\varepsilon^2), \tag{26}$$

where

$$\begin{aligned}\Delta P^{(1)} = \frac{\Delta_0}{\omega}\Big\{&(|c_1|^2-|c_2|^2)\xi_{\rm a}(\tau)\\ &-2{\rm Im}[c_1c_2^*]\left(\frac{1}{2}J_0(\zeta)\tau + \xi_{\rm s}(\tau)\right)\Big\}.\end{aligned} \tag{27}$$

The zeroth-order terms, $|c_1 \pm c_2|^2/2$, are constant in time, and the sub-half-cycle electron transfer from one nucleus to the other is represented by the higher-order terms. As shown

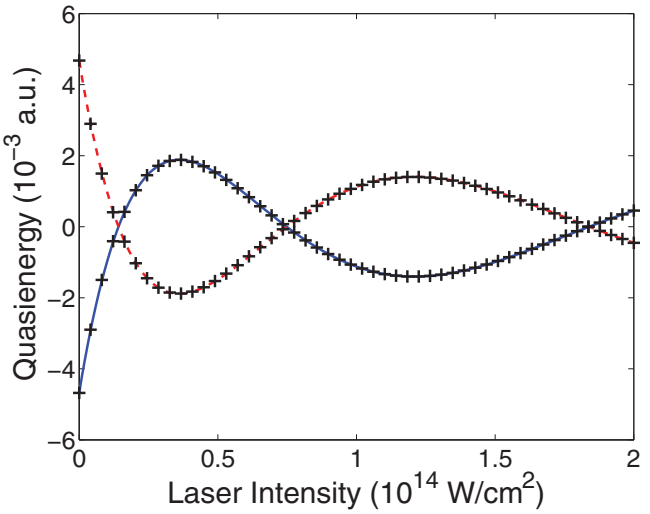

FIG. 3. (Color online) Quasienergies ϵ_1 and ϵ_2 calculated by numerically solving the eigenvalue Eq. (16) (black crosses) and from the formulas (17) and (18) (solid and dashed lines, respectively). The parameter values for the two-state model were taken from the 2D model. The laser wavelength was set at 800 nm.

above, for the present laser and molecular parameters, the local population dynamics can be analyzed using the terms up to the first order of the expansions.

The time instants at which either one of the local populations $|\langle \mathrm{L}|\Psi^{(2\mathrm{lev})}(\tau)\rangle|^2$ or $|\langle \mathrm{R}|\Psi^{(2\mathrm{lev})}(\tau)\rangle|^2$ is maximized are given by the condition

$$\frac{d}{d\tau}\Delta P^{(1)} = 0. \tag{28}$$

It can be shown that this is equivalent to

$$(|c_1|^2 - |c_2|^2)\sin[2\phi(\tau)] - 2\mathrm{Im}[c_1 c_2^*]\cos[2\phi(\tau)] = 0. \tag{29}$$

The left-hand side of this equation can be written as $\sin[2\phi(\tau)+\chi]$, where

$$\cos\chi = \frac{|c_1|^2 - |c_2|^2}{C}, \tag{30}$$

$$\sin\chi = -\frac{2\mathrm{Im}[c_1 c_2^*]}{C}, \tag{31}$$

$$C = \sqrt{(|c_1|^2 - |c_2|^2)^2 + 4(\mathrm{Im}[c_1 c_2^*])^2}. \tag{32}$$

Therefore, one of the local populations is maximized if $2\phi(\tau)+\chi$ is equal to an integer multiple of π. Using Eq. (21), we thus obtain that the electron is maximally localized at a proton at the time instants t_{loc} given by

$$A(t_{\mathrm{loc}}) = \frac{m\pi + \chi}{2d_{\mathrm{gu}}} + \tilde{A}, \quad \text{with } m \in \mathbb{Z}. \tag{33}$$

Furthermore, one can show that

$$\left.\frac{d^2\Delta P^{(1)}}{d\tau^2}\right|_{t=t_{\mathrm{loc}}} = (-1)^m \frac{C\Delta_0 d_{\mathrm{gu}}}{\omega^2} E(t_{\mathrm{loc}}). \tag{34}$$

This indicates that for those t_{loc} which correspond to odd m the electron is localized at the proton which is lower in the electric potential of the laser field.

These relations enable us to predict the timing of maximum electron localization in terms of the vector potential $A(t)$ if the dipole transition matrix element d_{gu} and the mixing angle of the Floquet states χ are known. We have shown previously how the value of χ can be determined experimentally by probing the IR-laser-driven H_2^+ with an attosecond XUV laser pulse [8].

In Figs. 1(d) and 2(d), the vector potential $A(t_{\mathrm{loc}})$ and the time instants of maximum localization, t_{loc}, according to Eq. (33), are indicated by the horizontal and vertical grid lines, respectively. The parameters Δ_0 and d_{gu} of the two-state model were set to those values of the 2D model. They correctly predict the transient localization of the electron in Figs. 1(c) and 2(b). For this prediction the value of χ was set to zero, which should be a good approximation as long as a long laser pulse of more than a few cycles duration is applied to the system prepared in the ground state. Under this condition, the system evolves into a single Floquet state $|\varphi_1^{\mathrm{F}}(\tau)\rangle$ [31,32].

Figure 4 shows the transient population transfer between $|\mathrm{L}\rangle$ and $|\mathrm{R}\rangle$ as given by the first-order terms of Eqs. (25) and (26) in a single Floquet state ($c_1 = 1$ and $c_2 = 0$) as a function of time and intensity. The results show that in a field of low intensity there is just one maximum of the localization at the peaks of the pulse [9]. On the other hand, in a more intense laser field there can be more than two time instants per half cycle at which the population localizes at one of the protons. Furthermore, please note that the electron localizes at different protons in different intensity regimes.

D. Static and subcycle electron localization

The expansions of the local populations in Eqs. (25) and (26) indicate that there are two modes of electron localization. One is the static localization represented by the zeroth-order terms, $|c_1 \pm c_2|^2/2$, and the other is the subcycle transient localization represented by the first-order terms, $\pm\Delta P^{(1)}$.

In the static localization, the electron densities at the two protons may become asymmetric for more than one cycle of the laser field. As the expression $|c_1 \pm c_2|^2/2$ suggests, this static localization appears when the two Floquet states $|\varphi_1^{\mathrm{F}}(\tau)\rangle$ and $|\varphi_2^{\mathrm{F}}(\tau)\rangle$ are superposed. Such a superposition can be created if a laser pulse of rapidly increasing envelope is applied to H_2^+ in one of the eigenstates, $|\mathrm{g}\rangle$ or $|\mathrm{u}\rangle$, or if the initial state of H_2^+ is prepared in a superposition of $|\mathrm{g}\rangle$ and $|\mathrm{u}\rangle$. This static mode of electron localization has been shown to generate even order harmonics [22,23,33] and also to contribute to enhanced ionization [14].

If a laser pulse is longer than a few cycles, the field may be well approximated as a cw field. Under this condition, the two Floquet states belong to different irreducible representations of the generalized parity symmetry [31,32]. As a result, if H_2^+ was initially in the $|\mathrm{g}\rangle$ (or $|\mathrm{u}\rangle$) state, it evolves into the single Floquet state $|\varphi_1^{\mathrm{F}}(\tau)\rangle$ ($|\varphi_2^{\mathrm{F}}(\tau)\rangle$) in the laser pulse, and hence $|c_1|^2 = 1$ and $|c_2|^2 = 0$ ($|c_1|^2 = 0$ and $|c_2|^2 = 1$). Therefore, at the zeroth order, the local populations $|\langle \mathrm{L}|\Psi^{(2\mathrm{lev})}\rangle|^2$ and $|\langle \mathrm{R}|\Psi^{(2\mathrm{lev})}\rangle|^2$ are both 1/2 and there is no localization. In contrast, the transient electron localization [10,11] and the related MIBs [8,9], are due to the first-order terms in the expansion and occur for any length of the pulse and initial state of the system.

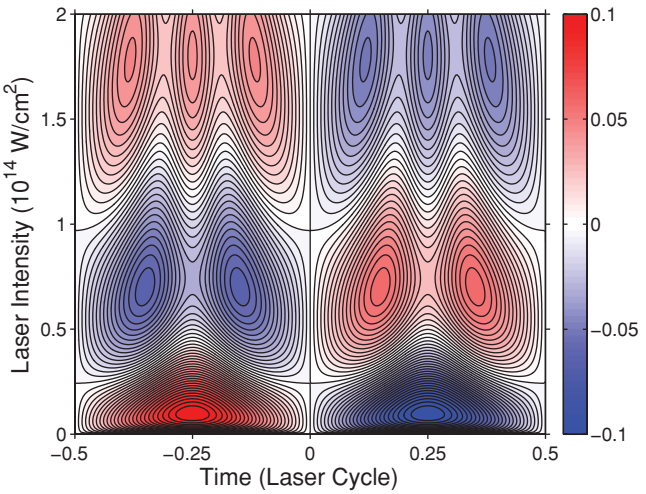

FIG. 4. (Color online) Population transfer $\Delta P^{(1)}$ from $|\mathrm{R}\rangle$ to $|\mathrm{L}\rangle$ in the single Floquet state ($c_1 = 1$ and $c_2 = 0$). The ground-state and first excited-state energies as well as the transition dipole of the 2D model at $R = 7$ were used to parametrize the two-level system. The laser wavelength was set equal to 800 nm.

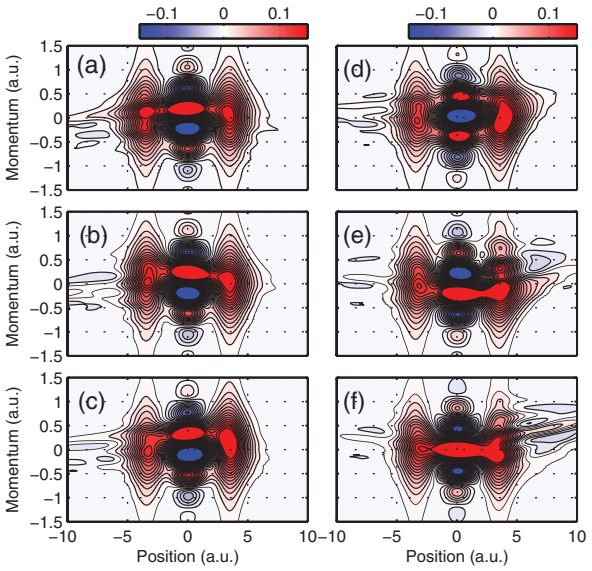

FIG. 5. (Color online) Time evolution of the Wigner distribution over a quarter cycle of the laser field for the 1D model: (a) $t = -0.500$, (b) -0.450, (c) -0.400, (d) -0.351, (e) -0.301, and (f) -0.251 laser cycles.

IV. SUBCYCLE-RESOLVED VIEW ON CREI

It is known that H_2^+ is ionized rapidly when it is stretched to internuclear distances of 5 to 12 a.u. during dissociation. This phenomenon, called CREI, has been predicted [15,33–37] and observed in experiments [38–41]. The mechanism has been understood as follows [15,33,38]: The strong electric field of the laser light lifts up the potential energy at one of the protons while decreasing it at the other proton, which results in an energy gap of about $E(t)R_0$. If the electronic states follow $E(t)$ adiabatically, at the intermediate internuclear distances the upper state lies above the internal potential barrier. Therefore, it is expected that from this state the electron wave packet is ionized efficiently. In this adiabatic picture, the populations of the upper and lower states are considered to be constant over one half cycle while the electric field points to one direction, and the ionization current is expected to be the strongest at the field maxima.

As discussed above, the first-order term in our Floquet analysis causes the subcycle electron localization, and the adiabatic picture of CREI partially breaks down on the ultrashort time scale. It is therefore important to reexamine another characteristics of CREI as well, namely, that the electron is ionized from the uphill potential well, in order to clarify the relation between MIB and CREI. This is difficult to see in the probability density in the position space shown in Fig. 1, but can be elucidated in the Wigner distribution [11,42].

Figure 5 shows six snapshots of the Wigner distribution of the 1D fixed-nuclei model taken over a quarter period of the laser field. The laser and molecular parameters are the same as used in Figs. 1 and 2. The Wigner distribution in Fig. 5(a) is taken when the electric field is zero and at this time the electron density is equally distributed at the two nuclei at $z = \pm R_0/2 = \pm 3.5$. The oscillatory structure along the momentum (p_z) axis for $z = 0$ appears due to the two-center interference effect. As pointed out in Ref. [11] this interference pattern is displaced by the vector potential $A(t)$.

It is the positive (red) part of the interference pattern which mediates the transfer of the electron probability density from one proton to the other. These structures are called momentum gates (MGs) [11]. In Fig. 5(a), there is a gate at about $p_z = 0.2$, through which the probability flows toward the positive z direction. As a result, the electron population at the right proton ($z = R_0/2$) increases during the time interval over which the snapshots in Figs. 5(a) to 5(c) are taken. At the same time, the MG is moved to larger p_z, and therefore the probability density transferred through this gate arrives at $z = R_0/2$ with higher momentum as time evolves. As a result, the probability density can escape more easily the attraction of the proton at $z = R_0/2$ and ionize to $z \to +\infty$ as captured in Fig. 5(d).

In the snapshots shown in Figs. 5(d) to 5(e), the transfer through the first MG decreases while transfer through another gate which moves from $p_z = -0.2$ [Fig. 5(d)] to $p_z = 0$ [Fig. 5(e)] becomes more prominent. This new gate transfers the probability density from $z = R_0/2$ to $z = -R_0/2$, forcing the probability density to climb up the laser electric potential. Due to this uphill transport, the ionization burst started at the time instant of Fig. 5(d) is ceased and the electron is partially delocalized again in the snapshot shown in Fig. 5(f). We can therefore conclude that the electron starts to be ionized from the uphill potential well and the multiple burst phenomenon can be understood as CREI modulated by the oscillating MGs. A detailed analysis of the gating effect in terms of the Bohmian trajectories has been given recently [9].

V. CONCLUSION

We confirmed that the previously reported MIBs in 1D models of H_2^+ are also present in a more realistic 2D model. By analyzing the two-state model in terms of the series expansion of Floquet states, we showed that the transient electron localization and MIBs in a half cycle are represented by the first-order term of the expansion and derived a simple condition to predict the instants of maximum localization and thus those of the MIBs. Our analysis of the sub-laser-cycle electron dynamics in H_2^+ refines the adiabatic view of CREI. We showed in the quantum phase space that the ionizing electron wave packets indeed start from the uphill potential well as in the traditional CREI picture, but that the transport from the uphill well to the downhill well is regulated by the MGs, thus leading to the multiple bursts of ionization on the ultrashort time scale.

ACKNOWLEDGMENTS

This work was supported by NSF.

[1] P. Agostini, F. Fabre, G. Mainfray, G. Petite, and N. K. Rahman, Phys. Rev. Lett. **42**, 1127 (1979).

[2] T. Popmintchev, M. C. Chen, P. Arpin, M. M. Murnane, and H. C. Kapteyn, Nat. Photon. **4**, 822 (2011).

[3] A. Becker, R. Dörner, and R. Moshammer, J. Phys. B **38**, S753 (2005).
[4] F. Krausz and M. Ivanov, Rev. Mod. Phys. **81**, 163 (2009).
[5] P. B. Corkum and F. Krausz, Nat. Phys. **3**, 381 (2007).
[6] M. Uiberacker *et al.*, Nature (London) **446**, 627 (2007).
[7] G. L. Yudin and M. Y. Ivanov, Phys. Rev. A **64**, 013409 (2001).
[8] N. Takemoto and A. Becker, Phys. Rev. Lett. **105**, 203004 (2010).
[9] N. Takemoto and A. Becker, J. Chem. Phys. **134**, 074309 (2011).
[10] I. Kawata, H. Kono, and Y. Fujimura, J. Chem. Phys. **110**, 11152 (1999).
[11] F. He, A. Becker, and U. Thumm, Phys. Rev. Lett. **101**, 213002 (2008).
[12] R. S. Mulliken, J. Chem. Phys. **7**, 20 (1939).
[13] L. Pauling, Proc. Natl. Acad. Sci. USA **25**, 577 (1939).
[14] T. Zuo and A. D. Bandrauk, Phys. Rev. A **52**, R2511 (1995).
[15] T. Seideman, M. Y. Ivanov, and P. B. Corkum, Phys. Rev. Lett. **75**, 2819 (1995).
[16] A. Santana, J. M. G. Llorente, and V. Delgado, J. Phys. B **34**, 2371 (2001).
[17] S. E. Koonin, K. T. R. Davies, V. Maruhn-Rezwani, H. Feldmeier, S. J. Krieger, and J. W. Negele, Phys. Rev. C **15**, 1359 (1977).
[18] K. C. Kulander, K. R. S. Devi, and S. E. Koonin, Phys. Rev. A **25**, 2968 (1982).
[19] M. W. J. Bromley and B. D. Esry, Phys. Rev. A **69**, 053620 (2004).
[20] K. C. Kulander, F. H. Mies, and K. J. Schafer, Phys. Rev. A **53**, 2562 (1996).
[21] R. Herman and R. F. Wallis, Astrophys. J. **123**, 353 (1956).
[22] M. Y. Ivanov, P. B. Corkum, and P. Dietrich, Laser Phys. **3**, 375 (1993).
[23] M. Y. Ivanov and P. B. Corkum, Phys. Rev. A **48**, 580 (1993).
[24] N. Moiseyev, Phys. Rep. **302**, 212 (1998).
[25] S.-I. Chu and D. A. Telnov, Phys. Rep. **390**, 1 (2004).
[26] H. Rottke, B. Wolff-Rottke, D. Feldmann, K. H. Welge, M. Dörr, R. M. Potvliege, and R. Shakeshaft, Phys. Rev. A **49**, 4837 (1994).
[27] T. Yasuike and K. Someda, Phys. Rev. A **66**, 053410 (2002).
[28] M. Plummer, J. McCann, and L. B. Madsen, Comput. Phys. Commun. **114**, 94 (1998).
[29] I. Maruyama, T. Sako, and K. Yamanouchi, J. Phys. B **37**, 3919 (2004).
[30] C. Lefebvre, T. T. Nguyen-Dang, and O. Atabek, Phys. Rev. A **75**, 023404 (2007).
[31] J. E. Avron, J. S. Howland, and B. Simon, Commun. Math. Phys. **128**, 497 (1990).
[32] M. Holthaus, Phys. Rev. Lett. **69**, 1596 (1992).
[33] T. Zuo, S. Chelkowski, and A. D. Bandrauk, Phys. Rev. A **48**, 3837 (1993).
[34] M. Vafaee and H. Sabzyan, J. Phys. B **37**, 4143 (2004).
[35] L.-Y. Peng, D. Dundas, J. F. McCann, K. T. Taylor, and I. D. Williams, J. Phys. B **36**, L295 (2003).
[36] M. Plummer and J. McCann, J. Phys. B **29**, 4625 (1996).
[37] S. Chelkowski, A. D. Bandrauk, A. Staudte, and P. B. Corkum, Phys. Rev. A **76**, 013405 (2007).
[38] K. Codling and L. Frasinski, J. Phys. B **26**, 783 (1993).
[39] G. N. Gibson, M. Li, C. Guo, and J. Neira, Phys. Rev. Lett. **79**, 2022 (1997).
[40] A. Staudte *et al.*, Phys. Rev. Lett. **98**, 073003 (2007).
[41] I. Ben Itzhak *et al.*, Phys. Rev. A **78**, 063419 (2008).
[42] E. Wigner, Phys. Rev. **40**, 749 (1932).